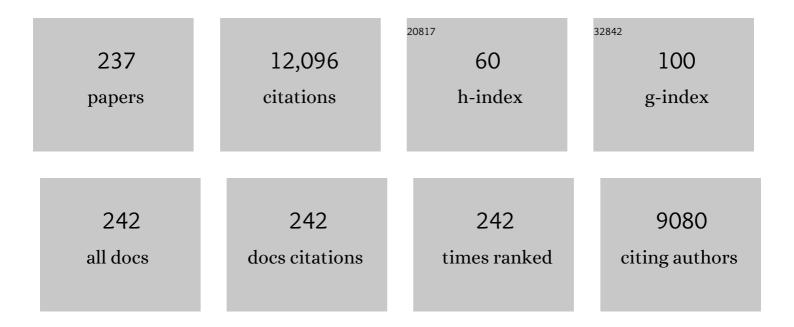
List of Publications by Year in descending order

Source: https://exaly.com/author-pdf/8533938/publications.pdf Version: 2024-02-01



IÃORC E LÃORERED

#	Article	lF	CITATIONS
1	MgZnCa glasses without clinically observable hydrogen evolution for biodegradable implants. Nature Materials, 2009, 8, 887-891.	27.5	775
2	Magnesium alloys for temporary implants in osteosynthesis: In vivo studies of their degradation and interaction with bone. Acta Biomaterialia, 2012, 8, 1230-1238.	8.3	506
3	Bulk metallic glasses. Intermetallics, 2003, 11, 529-540.	3.9	501
4	Design strategy for biodegradable Fe-based alloys for medical applicationsâ~†. Acta Biomaterialia, 2010, 6, 1705-1713.	8.3	432
5	On the in vitro and in vivo degradation performance and biological response of new biodegradable Mg–Y–Zn alloysâ~†. Acta Biomaterialia, 2010, 6, 1824-1833.	8.3	304
6	Biodegradable Fe-based alloys for use in osteosynthesis: Outcome of an in vivo study after 52weeks. Acta Biomaterialia, 2014, 10, 3346-3353.	8.3	211
7	Plasmon resonances of aluminum nanoparticles and nanorods. Journal of Applied Physics, 2008, 104, .	2.5	209
8	Deep-UV Surface-Enhanced Resonance Raman Scattering of Adenine on Aluminum Nanoparticle Arrays. Journal of the American Chemical Society, 2012, 134, 1966-1969.	13.7	207
9	In vivo degradation performance of micro-arc-oxidized magnesium implants: A micro-CT study in rats. Acta Biomaterialia, 2013, 9, 5411-5420.	8.3	193
10	Shearâ€Band Dynamics in Metallic Glasses. Advanced Functional Materials, 2015, 25, 2353-2368.	14.9	190
11	Propagation dynamics of individual shear bands during inhomogeneous flow in a Zr-based bulk metallic glass. Acta Materialia, 2011, 59, 3205-3213.	7.9	181
12	Random and exchange anisotropy in consolidated nanostructured Fe and Ni: Role of grain size and trace oxides on the magnetic properties. Physical Review B, 1998, 57, 2915-2924.	3.2	171
13	Magnetic Correlations in Nanostructured Ferromagnets. Physical Review Letters, 2000, 85, 1990-1993.	7.8	171
14	Aluminium carbide formation in interpenetrating graphite/aluminium composites. Materials Science & Engineering A: Structural Materials: Properties, Microstructure and Processing, 2007, 448, 1-6.	5.6	161
15	Thermodynamics, enthalpy relaxation and fragility of the bulk metallic glass-forming liquid Pd43Ni10Cu27P20. Acta Materialia, 2004, 52, 667-674.	7.9	150
16	Probing Shear-Band Initiation in Metallic Glasses. Physical Review Letters, 2011, 107, 185502.	7.8	135
17	Diffusion on Demand to Control Precipitation Aging: Application to Al-Mg-Si Alloys. Physical Review Letters, 2014, 112, 225701.	7.8	132
18	Processing and microstructure–property relations of high-strength low-alloy (HSLA) Mg–Zn–Ca alloys. Acta Materialia, 2015, 98, 423-432.	7.9	126

JöRG F LöFFLER

#	Article	IF	CITATIONS
19	Model for decomposition and nanocrystallization of deeply undercooled Zr41.2Ti13.8Cu12.5Ni10Be22.5. Applied Physics Letters, 2000, 76, 3394-3396.	3.3	121
20	Room-temperature creep and structural relaxation of Mg–Cu–Y metallic glasses. Acta Materialia, 2008, 56, 3777-3785.	7.9	118
21	Degradation performance of biodegradable FeMnC(Pd) alloys. Materials Science and Engineering C, 2013, 33, 1882-1893.	7.3	118
22	High-Strength Low-Alloy (HSLA) Mg–Zn–Ca Alloys with Excellent Biodegradation Performance. Jom, 2014, 66, 566-572.	1.9	115
23	Bulk metallic glass formation in Zr–Cu–Fe–Al alloys. Applied Physics Letters, 2005, 86, 241909.	3.3	113
24	Stick–slip behavior of serrated flow during inhomogeneous deformation of bulk metallic glasses. Acta Materialia, 2010, 58, 3742-3750.	7.9	110
25	Constitutive model for inhomogeneous flow in bulk metallic glasses. Acta Materialia, 2009, 57, 881-892.	7.9	109
26	Cytotoxicity of Zr-based bulk metallic glasses. Intermetallics, 2006, 14, 729-734.	3.9	107
27	Assessing the degradation performance of ultrahigh-purity magnesium in vitro and in vivo. Corrosion Science, 2015, 91, 29-36.	6.6	106
28	Interface formation in aluminium–aluminium compound casting. Acta Materialia, 2008, 56, 3036-3043.	7.9	105
29	Stick-slip dynamics and recent insights into shear banding in metallic glasses. Journal of Materials Research, 2011, 26, 1453-1463.	2.6	105
30	Grain-boundary atomic structure in nanocrystalline palladium from x-ray atomic distribution functions. Physical Review B, 1995, 52, 7076-7093.	3.2	104
31	Laser additive manufacturing of biodegradable magnesium alloy WE43: A detailed microstructure analysis. Acta Biomaterialia, 2019, 98, 36-49.	8.3	103
32	Shear striations and deformation kinetics in highly deformed Zr-based bulk metallic glasses. Acta Materialia, 2008, 56, 4635-4646.	7.9	101
33	Non-linear alignment dynamics in suspensions of platelets under rotating magnetic fields. Soft Matter, 2012, 8, 7604-7609.	2.7	101
34	Formation of Bulk Metallic Glasses and Their Composites. MRS Bulletin, 2007, 32, 624-628.	3.5	100
35	Time–temperature–transformation diagram and microstructures of bulk glass forming Pd40Cu30Ni10P20. Applied Physics Letters, 2000, 77, 681-683.	3.3	96
36	Microstructural studies of crystallization of a Zr-based bulk metallic glass. Acta Materialia, 2003, 51, 4045-4057.	7.9	96

#	Article	IF	CITATIONS
37	Tensile properties of glassy MgZnCa wires and reliability analysis using Weibull statistics. Acta Materialia, 2009, 57, 3223-3231.	7.9	93
38	Long-term in vivo degradation behavior and near-implant distribution of resorbed elements for magnesium alloys WZ21 and ZX50. Acta Biomaterialia, 2016, 42, 440-450.	8.3	82
39	High Aspect Ratio Plasmonic Nanostructures for Sensing Applications. ACS Nano, 2011, 5, 6374-6382.	14.6	80
40	The influence of biodegradable magnesium implants on the growth plate. Acta Biomaterialia, 2018, 66, 109-117.	8.3	80
41	Design strategy for microalloyed ultra-ductile magnesium alloys. Philosophical Magazine Letters, 2009, 89, 377-390.	1.2	78
42	Experimental investigation and thermodynamic assessment of the Cu–Sn–Ti ternary system. Calphad: Computer Coupling of Phase Diagrams and Thermochemistry, 2011, 35, 82-94.	1.6	76
43	Rational design of a lean magnesium-based alloy with high age-hardening response. Acta Materialia, 2018, 158, 214-229.	7.9	76
44	Existence of multiple critical cooling rates which generate different types of monolithic metallic glass. Nature Communications, 2019, 10, 1337.	12.8	76
45	Ferromagnetic resonance and magnetic characteristics of intact magnetosome chains in Magnetospirillum gryphiswaldense. Earth and Planetary Science Letters, 2008, 270, 200-208.	4.4	75
46	Atomic structure of nanocrystalline metals studied by diffraction techniques and EXAFS. Scripta Materialia, 1995, 6, 105-114.	0.5	74
47	Structure and properties of a hypoeutectic chromium steel processed in the semi-solid state. Acta Materialia, 2006, 54, 2727-2734.	7.9	74
48	Negative strain rate sensitivity in bulk metallic glass and its similarities with the dynamic strain aging effect during deformation. Applied Physics Letters, 2006, 89, 091918.	3.3	73
49	<i>In-situ</i> probing of metallic glass formation and crystallization upon heating and cooling via fast differential scanning calorimetry. Applied Physics Letters, 2014, 104, .	3.3	73
50	Magnesium from bioresorbable implants: Distribution and impact on the nano- and mineral structure of bone. Biomaterials, 2016, 76, 250-260.	11.4	73
51	Recrystallization behavior, microstructure evolution and mechanical properties of biodegradable Fe–Mn–C(–Pd) TWIP alloys. Acta Materialia, 2012, 60, 2746-2756.	7.9	71
52	Ultrafast artificial aging of Al–Mg–Si alloys. Scripta Materialia, 2016, 112, 148-151.	5.2	70
53	Solid–solid phase transitions via melting in metals. Nature Communications, 2016, 7, 11113.	12.8	69
54	Influence of trace impurities on the in vitro and in vivo degradation of biodegradable Mg–5Zn–0.3Ca alloys. Acta Biomaterialia, 2015, 23, 347-353.	8.3	67

#	Article	IF	CITATIONS
55	Stress corrosion cracking and corrosion fatigue characterisation of MgZn1Ca0.3 (ZX10) in a simulated physiological environment. Journal of the Mechanical Behavior of Biomedical Materials, 2017, 65, 634-643.	3.1	66
56	Temperature-dependent shear band dynamics in a Zr-based bulk metallic glass. Applied Physics Letters, 2010, 96, .	3.3	65
57	Crystallization of bulk amorphous Zr–Ti(Nb)–Cu–Ni–Al. Applied Physics Letters, 2000, 77, 525-527.	3.3	64
58	Deformation kinetics in Zr-based bulk metallic glasses and its dependence on temperature and strain-rate sensitivity. Philosophical Magazine Letters, 2007, 87, 695-704.	1.2	63
59	On the microstructure and properties of 100Cr6 steel processed in the semi-solid state. Acta Materialia, 2007, 55, 6553-6560.	7.9	63
60	Electric and magnetic resonances in arrays of coupled gold nanoparticle in-tandem pairs. Optics Express, 2008, 16, 13287.	3.4	63
61	On the origin of primary ½ a0 <111> and a0 <100> loops in irradiated Fe(Cr) alloys. Acta Materialia, 2017, 133, 427-439.	7.9	63
62	The role of zinc in the biocorrosion behavior of resorbable Mg‒Zn‒Ca alloys. Acta Biomaterialia, 2019, 100, 398-414.	8.3	63
63	Structured nanoscale metallic glass fibres with extreme aspect ratios. Nature Nanotechnology, 2020, 15, 875-882.	31.5	59
64	Crystallization of amorphous Cu[sub 47]Ti[sub 34]Zr[sub 11]Ni[sub 8]. Journal of Applied Physics, 2001, 89, 1573.	2.5	58
65	Single shear-band plasticity in a bulk metallic glass at cryogenic temperatures. Scripta Materialia, 2012, 66, 231-234.	5.2	57
66	Size-dependent diffusion controls natural aging in aluminium alloys. Nature Communications, 2019, 10, 4746.	12.8	57
67	Deformation behavior of silver submicrometer-pillars prepared by nanoimprinting. Philosophical Magazine, 2009, 89, 869-884.	1.6	56
68	The Boson peak of model glass systems and its relation to atomic structure. European Physical Journal B, 2012, 85, 1.	1.5	52
69	Shear-band arrest and stress overshoots during inhomogeneous flow in a metallic glass. Applied Physics Letters, 2012, 100, .	3.3	52
70	Comparison of a resorbable magnesium implant in small and large growing-animal models. Acta Biomaterialia, 2018, 78, 378-386.	8.3	52
71	3D Printing of Salt as a Template for Magnesium with Structured Porosity. Advanced Materials, 2019, 31, e1903783.	21.0	52
72	Metal direct nanoimprinting for photonics. Microelectronic Engineering, 2008, 85, 419-424.	2.4	51

#	Article	IF	CITATIONS
73	Thermodynamic Assessment of the Sn–Ti System. Monatshefte Für Chemie, 2005, 136, 1921-1930.	1.8	49
74	Influence of grain size and oxidation on the magnetic properties of nanostructured Fe and Ni. Scripta Materialia, 1997, 9, 523-526.	0.5	48
75	Devitrification of the Zr41.2Ti13.8Cu12.5Ni10.0Be22.5 bulk metallic glass studied by XRD, SANS, and NMR. Journal of Non-Crystalline Solids, 2003, 317, 118-122.	3.1	47
76	Experimental study of the Fe–Ni–Ti system. Intermetallics, 2010, 18, 374-384.	3.9	47
77	Magnetization processes in nanostructured metals and small-angle neutron scattering. Physical Review B, 2005, 71, .	3.2	45
78	Critical Poisson ratio for room-temperature embrittlement of amorphous Mg85Cu5Y10. Philosophical Magazine Letters, 2007, 87, 383-392.	1.2	45
79	Bulk metallic glass–graphite composites. Scripta Materialia, 2007, 56, 1079-1082.	5.2	43
80	Deformation behavior of gold nano-pillars prepared by nanoimprinting and focused ion-beam milling. Acta Materialia, 2011, 59, 2180-2192.	7.9	43
81	A lean magnesium–zinc–calcium alloy ZX00 used for bone fracture stabilization in a large growing-animal model. Acta Biomaterialia, 2020, 113, 646-659.	8.3	43
82	Crossover in the magnetic properties of nanostructured metals. Materials Science & Engineering A: Structural Materials: Properties, Microstructure and Processing, 2001, 304-306, 1050-1054.	5.6	42
83	Interface formation between liquid and solid Mg alloys—An approach to continuously metallurgic joining of magnesium parts. Materials Science & Engineering A: Structural Materials: Properties, Microstructure and Processing, 2010, 527, 2274-2279.	5.6	42
84	Process-controlled suppression of natural aging in an Al–Mg–Si alloy. Scripta Materialia, 2014, 89, 53-56.	5.2	42
85	Microstructural development during final-stage sintering of nanostructured zirconia based ceramics. Materials Science & Engineering A: Structural Materials: Properties, Microstructure and Processing, 2000, 281, 68-74.	5.6	41
86	Icosahedral superclusters in <mml:math xmlns:mml="http://www.w3.org/1998/Math/MathML"> <mml:mrow> <mml:msub> <mml:mi> Cu </mml:mi> <mm glass. Physical Review B, 2014, 90, .</mm </mml:msub></mml:mrow></mml:math 	:mn 3 £4 </td <td>mmlaøın></td>	mm laø ın>
87	Surface-induced vacancy loops and damage dispersion in irradiated Fe thin films. Acta Materialia, 2015, 101, 22-30.	7.9	38
88	Time-resolved measurement of shear-band temperature during serrated flow in a Zr-based metallic glass. Acta Materialia, 2016, 115, 468-474.	7.9	38
89	Characterization, mechanical properties and dimensional accuracy of a Zr-based bulk metallic glass manufactured via laser powder-bed fusion. Materials and Design, 2021, 199, 109400.	7.0	38
90	Magnetoelastic coupling in the triangular lattice antiferromagnet <mml:math xmlns:mml="http://www.w3.org/1998/Math/MathML" dicplay="inling"><mml:mrow><mml:mrow><mml:mrow><mml:mtext></mml:mtext></mml:mrow><mml:mtext></mml:mtext></mml:mrow><mml:mtext></mml:mtext><td>mn³2/m</td><td>ml: 37</td></mml:mrow></mml:math 	mn ³ 2/m	ml: 37

⁹⁰ display="inline"><mml:mrow><mml:msub><mml:mrow><mml:mtext>CuCrS</mml:mtext></mml:mrow><mml:mn>22</mml:mn>2
Physical Review B, 2009, 80, .

JöRG F LöFFLER

#	Article	IF	CITATIONS
91	Fluxing of Pd–Si–Cu bulk metallic glass and the role of cooling rate and purification. Acta Materialia, 2014, 71, 145-152.	7.9	37
92	On the understanding of the effects of sample size on the variability in fracture toughness of bulk metallic glasses. Acta Materialia, 2017, 126, 494-506.	7.9	37
93	Metastable quasicrystal-induced nucleation in a bulk glass-forming liquid. Proceedings of the National Academy of Sciences of the United States of America, 2018, 115, 6123-6128.	7.1	37
94	Precipitation hardening of biodegradable Fe–Mn–Pd alloys. Acta Materialia, 2011, 59, 981-991.	7.9	36
95	Reverse α′→γ transformation mechanisms of martensitic Fe–Mn and age-hardenable Fe–Mn–Pd alloys fast and slow continuous heating. Acta Materialia, 2014, 72, 99-109.	upon	35
96	Towards refining microstructures of biodegradable magnesium alloy WE43 by spark plasma sintering. Acta Biomaterialia, 2019, 98, 67-80.	8.3	35
97	On the Immersion Testing of Degradable Implant Materials in Simulated Body Fluid: Active pH Regulation Using CO ₂ . Advanced Engineering Materials, 2013, 15, 434-441.	3.5	34
98	Local structural excitations in model glasses. Physical Review B, 2014, 89, .	3.2	34
99	Influence of decomposition on the thermal stability of undercooled Zr-Ti-Cu-Ni-Al alloys. Scripta Materialia, 2001, 44, 1269-1273.	5.2	33
100	Discrete deformation in amorphous metals: anin situSEM indentation study. Philosophical Magazine, 2006, 86, 5715-5728.	1.6	33
101	Characterization of bulk metallic glasses via fast differential scanning calorimetry. Thermochimica Acta, 2014, 590, 84-90.	2.7	33
102	Crystal-Like Rearrangements of Icosahedra in Simulated Copper-Zirconium Metallic Glasses and their Effect on Mechanical Properties. Physical Review Letters, 2015, 115, 165501.	7.8	32
103	Alloy design strategies for sustained ductility in Mg-based amorphous alloys – Tackling structural relaxation. Acta Materialia, 2016, 103, 735-745.	7.9	32
104	Monopole-Induced Emergent Electric Fields in Ferromagnetic Nanowires. Physical Review Letters, 2018, 121, 097202.	7.8	32
105	Structural analysis of rapidly solidified Mg–Cu–Y glasses during room-temperature embrittlement. Philosophical Magazine, 2009, 89, 233-248.	1.6	30
106	Tribological properties of graphite- and ZrC-reinforced bulk metallic glass composites. Intermetallics, 2007, 15, 1228-1236.	3.9	29
107	Reaction of bone nanostructure to a biodegrading Magnesium WZ21 implant – A scanning small-angle X-ray scattering time study. Acta Biomaterialia, 2016, 31, 448-457.	8.3	29
108	Biocorrosion Zoomed In: Evidence for Dealloying of Nanometric Intermetallic Particles in Magnesium Alloys. Advanced Materials, 2019, 31, e1903080.	21.0	29

#	Article	IF	CITATIONS
109	Magnetic correlations in nanostructured metals and an extended random-anisotropy model. Journal of Applied Physics, 1999, 85, 5187-5189.	2.5	28
110	Concentration and temperature dependence of decomposition in supercooled liquid alloys. Journal of Applied Crystallography, 2000, 33, 500-503.	4.5	28
111	Experimental investigation of the Cu–Ti–Zr system at 800°C. Intermetallics, 2007, 15, 1666-1671.	3.9	28
112	Biodegradable wound-closing devices for gastrointestinal interventions: Degradation performance of the magnesium tip. Materials Science and Engineering C, 2011, 31, 1098-1103.	7.3	28
113	Compositional dependence of shear-band dynamics in the Zr–Cu–Al bulk metallic glass system. Applied Physics Letters, 2014, 104, 101910.	3.3	28
114	Dynamic properties of major shear bands in Zr–Cu–Al bulk metallic glasses. Acta Materialia, 2015, 96, 428-436.	7.9	28
115	Enhancement of the intrinsic fluorescence of adenine using aluminum nanoparticle arrays. Optics Express, 2015, 23, 24719.	3.4	28
116	Critical crystallization properties of an industrial-grade Zr-based metallic glass used in additive manufacturing. Scripta Materialia, 2021, 199, 113861.	5.2	28
117	Immunological Response to Biodegradable Magnesium Implants. Jom, 2014, 66, 573-579.	1.9	27
118	Exceptional Strengthening of Biodegradable Mg-Zn-Ca Alloys through High Pressure Torsion and Subsequent Heat Treatment. Materials, 2019, 12, 2460.	2.9	26
119	Stacking-fault mediated plasticity and strengthening in lean, rare-earth free magnesium alloys. Acta Materialia, 2021, 211, 116877.	7.9	26
120	Silver high-aspect-ratio micro- and nanoimprinting for optical applications. Applied Physics Letters, 2009, 94, .	3.3	25
121	Large-scale synthesis of defined cobalt nanoparticles and magnetic metal–polymer composites. Nanoscale, 2009, 1, 374.	5.6	25
122	Segregation-driven exceptional twin-boundary strengthening in lean Mg–Zn–Ca alloys. Acta Materialia, 2022, 229, 117746.	7.9	25
123	Characterization of nanocrystalline palladium by x-ray atomic density distribution functions. Scripta Materialia, 1995, 6, 567-570.	0.5	24
124	Crystallization of Mg–Al and Al-based metallic liquids under ultra-high gravity. Intermetallics, 2002, 10, 1167-1175.	3.9	24
125	Crystallization of metallic glasses under the influence of high density dc currents. Journal of Applied Physics, 2004, 95, 2896-2899.	2.5	24
126	Structure and mechanical properties of bulk glass-forming Ni–Nb–Sn alloys. Scripta Materialia, 2006, 54, 187-190.	5.2	24

#	Article	IF	CITATIONS
127	Metallic foams from nanoparticle-stabilized wet foams and emulsions. Journal of Materials Chemistry, 2012, 22, 820-823.	6.7	24
128	Towards deep-UV surface-enhanced resonance Raman spectroscopy of explosives: ultrasensitive, real-time and reproducible detection of TNT. Analyst, The, 2015, 140, 5671-5677.	3.5	24
129	Skyrmion oscillations in magnetic nanorods with chiral interactions. Physical Review B, 2017, 95, .	3.2	24
130	Crystallization pathways of deeply undercooled Zr-Ti-Cu-Ni-Be melts. Scripta Materialia, 2001, 44, 1251-1255.	5.2	23
131	Random anisotropy and domain-wall pinning process in the magnetic properties of rapidly quenched Nd60Fe30Al10. Applied Physics Letters, 2003, 82, 721-723.	3.3	23
132	Metallic glass/polymer composites by co-processing at similar viscosities. Scripta Materialia, 2007, 56, 289-292.	5.2	23
133	Free-volume dependent pressure sensitivity of Zr-based bulk metallic glass. Journal of Materials Research, 2009, 24, 2697-2704.	2.6	23
134	Magnetic metamaterials in the blue range using aluminum nanostructures. Optics Letters, 2010, 35, 1656.	3.3	23
135	In Vivo Performance and Structural Relaxation of Biodegradable Bone Implants Made from MgZnCa Bulk Metallic Glasses. Advanced Engineering Materials, 2012, 14, B357.	3.5	23
136	Effectiveness of hydrogen microalloying in bulk metallic glass design. Acta Materialia, 2015, 99, 415-421.	7.9	23
137	Local structural excitations in model glass systems under applied load. Physical Review B, 2016, 93, .	3.2	23
138	Development of magnetic Fe-based metallic glasses without metalloids. Journal of Applied Physics, 2006, 99, 023908.	2.5	22
139	Comparison of the Decomposition and Crystallization Behavior of Zr and Pd Based Bulk Amorphous Alloys. Materials Science Forum, 2000, 343-346, 179-184.	0.3	21
140	Thermodynamics of polymorphism in a bulk metallic glass: Heat capacity measurements by fast differential scanning calorimetry. Thermochimica Acta, 2020, 685, 178518.	2.7	21
141	Corrosion properties of glassy Mg70Al15Ga15 in 0.1M NaCl solution. Intermetallics, 2009, 17, 811-817.	3.9	20
142	Magneto-electronic coupling in modulated defect-structures of natural Fe1â^' <i>x</i> S. Journal of Applied Physics, 2015, 118, .	2.5	20
143	Positron annihilation study of nanocrystalline iron. Scripta Materialia, 1999, 12, 1059-1062.	0.5	19
144	Abrasive waterjet machining of three-dimensional structures from bulk metallic glasses and comparison with other techniques, Journal of Materials Research, 2012, 27, 1187-1192	2.6	19

#	Article	IF	CITATIONS
145	Model for decomposition and crystallization of Zr-based bulk amorphous alloys near the glass transition. Materials Science & Engineering A: Structural Materials: Properties, Microstructure and Processing, 2001, 304-306, 670-673.	5.6	18
146	Hydrogen microalloying as a viable strategy for enhancing the glass-forming ability of Zr-based bulk metallic glasses. Scripta Materialia, 2015, 103, 53-56.	5.2	18
147	Additive manufacturing of a precious bulk metallic glass. Applied Materials Today, 2021, 24, 101080.	4.3	18
148	Nanoscale characterization of magnetic properties in nanostructured Fe, Ni and Co by small-angle neutron scattering. Scripta Materialia, 1997, 9, 331-334.	0.5	17
149	Effective temperature dynamics of shear bands in metallic glasses. Physical Review E, 2014, 90, 062405.	2.1	17
150	Exceptionally broad bulk metallic glass formation in the Mg–Cu–Yb system. Acta Materialia, 2017, 128, 188-196.	7.9	17
151	Atom Probe Tomography Study of Asâ€Quenched Al–Mg–Si Alloys. Advanced Engineering Materials, 2017, 19, 1600668.	3.5	17
152	Bulk metallic glass casting investigated using high-speed infrared monitoring and complementary fast scanning calorimetry. Acta Materialia, 2018, 151, 416-423.	7.9	17
153	Recent progress in the area of bulk metallic glasses. International Journal of Materials Research, 2006, 97, 225-233.	0.8	16
154	The influence of two common sterilization techniques on the corrosion of Mg and its alloys for biomedical applications. Journal of Biomedical Materials Research - Part B Applied Biomaterials, 2018, 106, 1907-1917.	3.4	16
155	Implant degradation of low-alloyed Mg–Zn–Ca in osteoporotic, old and juvenile rats. Acta Biomaterialia, 2022, 147, 427-438. Interaction-Induced Partitioning and Magnetization Jumps in the Mixed-Spin Oxide <mml:math< td=""><td>8.3</td><td>16</td></mml:math<>	8.3	16
156	xmlns:mml="http://www.w3.org/1998/Math/MathML" display="inline"> <mml:msub><mml:mi>FeTiO</mml:mi><mml:mn>3</mml:mn></mml:msub> <mml:mtext mathvariant="normal">â^`<mml:msub><mml:mi>Fe</mml:mi><mml:mn>2</mml:mn>mathvariant="normal">O<mml:mn>3</mml:mn></mml:msub>. Physical Review</mml:mtext 	> < 7.8 ml:ms	sub ¹⁵ <mml:m< td=""></mml:m<>
157	Letters, 2011, 107, 057202. Domain-wall dynamics in 4C pyrrhotite at low temperature. Geophysical Journal International, 2013, 195, 192-199.	2.4	15
158	Atomic-scale characterization of prior austenite grain boundaries in Fe–Mn-based maraging steel using site-specific atom probe tomography. Acta Materialia, 2014, 73, 215-226.	7.9	15
159	The detrimental effect of flux-induced boron alloying in Pd–Si–Cu bulk metallic glasses. Applied Physics Letters, 2015, 106, .	3.3	15
160	Grain-size dependence of intergranular magnetic correlations in nanostructured metals. Journal of Applied Crystallography, 2000, 33, 451-455.	4.5	14
161	Structural properties of determined from high-resolution synchrotron powder diffraction. Journal of Solid State Chemistry, 2009, 182, 1188-1192.	2.9	14
162	Variable defect structures cause the magnetic low-temperature transition in natural monoclinic pyrrhotite. Geophysical Journal International, 2016, 204, 961-967.	2.4	14

#	Article	IF	CITATIONS
163	Unconventional magnetization textures and domain-wall pinning in Sm–Co magnets. Scientific Reports, 2020, 10, 21209.	3.3	14
164	3D nanoscale analysis of bone healing around degrading Mg implants evaluated by X-ray scattering tensor tomography. Acta Biomaterialia, 2021, 134, 804-817.	8.3	14
165	Structural influence on atomic hopping and electronic states of Pd-based bulk metallic glasses. Applied Physics Letters, 2005, 86, 072104.	3.3	13
166	Shear-band propagation in fully amorphous and partially crystallized Mg-based alloys studied by nanoindentation and transmission electron microscopy. Journal of Alloys and Compounds, 2007, 434-435, 48-51.	5.5	13
167	Slow dynamics and field-induced transitions in a mixed-valence oxide solid solution. Physical Review B, 2011, 83, .	3.2	13
168	Tunable terahertz oscillation arising from Bloch-point dynamics in chiral magnets. Physical Review Research, 2020, 2, .	3.6	13
169	High-temperature centrifugation: a tool for finding eutectic compositions in multicomponent alloys. Applied Physics Letters, 2002, 81, 4159-4161.	3.3	12
170	Interface Reactions of Al and Binary Al-Alloys on Mild Steel Substrates in Controlled Atmosphere. Materials Science Forum, 2006, 519-521, 1157-1162.	0.3	12
171	High-purity amorphous Zr52.5Cu17.9Ni14.6Al10Ti5 powders via mechanical amorphization of crystalline pre-alloys. Materials Science & Engineering A: Structural Materials: Properties, Microstructure and Processing, 2006, 418, 236-240.	5.6	12
172	Effect of microalloying on the glass-forming ability of Cu60Zr30Ti10 bulk metallic glass. Journal of Non-Crystalline Solids, 2007, 353, 4218-4222.	3.1	12
173	µXRF Elemental Mapping of Bioresorbable Magnesium-Based Implants in Bone. Materials, 2016, 9, 811.	2.9	12
174	Ordered defects in Fe1â^' <i>x</i> S generate additional magnetic anisotropy symmetries. Journal of Applied Physics, 2018, 123, .	2.5	12
175	xmlns:mml="http://www.w3.org/1998/Math/MathML" display="inline"> <mml:msub><mml:mrow /><mml:mn>3</mml:mn></mml:mrow </mml:msub> and adjustable magnetic configuration in Fe(III)-doped FeTiO <mml:math <br="" xmlns:mml="http://www.w3.org/1998/Math/MathML">display="inline"><mml:msub><mml:mrow></mml:mrow><mml:mn>3</mml:mn></mml:msub></mml:math> . Physical	3.2	11
176	Review B, 2012, 86, . Equilibrium ternary intermetallic phase in the Mg–Zn–Ca system. Journal of Materials Research, 2016, 31, 2147-2155.	2.6	11
177	Multistep Crystallization and Melting Pathways in the Freeâ€Energy Landscape of a Au–Si Eutectic Alloy. Advanced Science, 2020, 7, 1903544.	11.2	11
178	Kinetics of structure formation in the vicinity of the glass transition. Acta Materialia, 2022, 226, 117630.	7.9	11
179	Scaling Behavior of Individual Nanoparticle Plasmon Resonances. Journal of Physical Chemistry C, 2015, 119, 6138-6147.	3.1	10
180	Crystallization of Bulk Glass Forming Pd-Based Melts, Materials Science Forum, 2001, 360-362, 79-84	0.3	9

#	Article	IF	CITATIONS
181	Processing of metallic glass-forming liquids under ultra-high gravity. Materials Science & Engineering A: Structural Materials: Properties, Microstructure and Processing, 2004, 375-377, 341-345.	5.6	9
182	Electron-band theory inspired design of magnesium–precious metal bulk metallic glasses with high thermal stability and extended ductility. Scientific Reports, 2017, 7, 3400.	3.3	9
183	Palladiumâ€Based Metallic Glass with High Thrombogenic Resistance for Bloodâ€Contacting Medical Devices. Advanced Functional Materials, 2022, 32, 2108256.	14.9	9
184	Structural and chemical characterization of the hardening phase in biodegradable Fe–Mn–Pd maraging steels. Journal of Materials Research, 2014, 29, 1069-1076.	2.6	8
185	Monotropic polymorphism in a glass-forming metallic alloy. Journal of Physics Condensed Matter, 2018, 30, 234002.	1.8	8
186	Collective antiskyrmion-mediated phase transition and defect-induced melting in chiral magnetic films. Scientific Reports, 2018, 8, 16675.	3.3	8
187	Cation diffusion patterns across the magneto-structural transition in Fe7S8. Physical Chemistry Chemical Physics, 2019, 21, 13040-13046.	2.8	8
188	Assessing continuous casting of precious bulk metallic glasses. Journal of Non-Crystalline Solids, 2019, 521, 119120.	3.1	8
189	The Besnus Transition in Singleâ€Domain 4C Pyrrhotite. Geochemistry, Geophysics, Geosystems, 2019, 20, 5216-5224.	2.5	8
190	Soft-magnetic materials characterized using a superconducting solenoid as magnetic source. Applied Physics Letters, 2008, 92, 082501.	3.3	7
191	Microstructural Changes of Vacuum Interrupter Contact Materials Caused by Switching Operations. , 2010, , .		7
192	Monte Carlo study of partitioning mechanisms in mixed-spin Ising systems. Physical Review B, 2011, 84, .	3.2	7
193	Competitive and cooperative anisotropy in magnetic nanocrystal chains of magnetotactic bacteria. Journal of Applied Physics, 2016, 120, 083901.	2.5	7
194	The relation between local structural distortion and the low-temperature magnetic anomaly in Fe ₇ S ₈ . Journal of Physics Condensed Matter, 2018, 30, 425803.	1.8	7
195	Torque analysis of incoherent spin rotation in the presence of ordered defects. Applied Physics Letters, 2018, 112, 202404.	3.3	7
196	Atom Probe Tomography Investigations of Modified Early Stage Clustering in Si-Containing Aluminum Alloys. Acta Physica Polonica A, 2015, 128, 643-647.	0.5	7
197	Eutectic isolation in Mg-Al-Cu-Li(-Y) alloys by centrifugal processing. Philosophical Magazine, 2003, 83, 2797-2813.	1.6	6
198	Phase separation and microstructure controlled magnetic properties of rapidly quenched Nd60Fe30Al10. Materials Science & Engineering A: Structural Materials: Properties, Microstructure and Processing, 2004, 375-377, 1027-1031.	5.6	6

#	Article	IF	CITATIONS
199	Synthesis of magnetic Fe-based bulk metallic glasses starting from the Fe–Cr–Co system. Journal of Applied Physics, 2007, 101, 013909.	2.5	6
200	Deformation kinetics of Zr-based bulk metallic glasses—Temperature and strain rate influences on shear banding. Journal of Alloys and Compounds, 2010, 495, 341-344.	5.5	6
201	Fe-Ti-O exchange at high temperature and thermal hysteresis. Geophysical Journal International, 2011, 185, 647-652.	2.4	6
202	Reprint of: Characterization of bulk metallic glasses via fast differential scanning calorimetry. Thermochimica Acta, 2015, 603, 46-52.	2.7	6
203	Löffler, Braun, and Wagner Reply:. Physical Review Letters, 2001, 87, .	7.8	5
204	Processing of diamond-reinforced bulk metallic glass composites. Materials Science & Engineering A: Structural Materials: Properties, Microstructure and Processing, 2007, 447, 298-302.	5.6	5
205	Experimental study of the FeAl–NiAl–TiAl section. Intermetallics, 2012, 23, 80-90.	3.9	5
206	On the Magnetism Behind the Besnus Transition in Monoclinic Pyrrhotite. Journal of Geophysical Research: Solid Earth, 2018, 123, 6236-6246.	3.4	5
207	Temperature dependence of magnetization processes in Sm(Co, Fe, Cu, Zr) <i>z</i> magnets with different nanoscale microstructures. Journal of Applied Physics, 2021, 129, .	2.5	5
208	Magnetization response in bulk nanostructured magnets. Materials Science & Engineering A: Structural Materials: Properties, Microstructure and Processing, 2007, 449-451, 407-413.	5.6	4
209	High-throughput fabrication of nanoantennae over large areas for biosensing and nanospectroscopy. Applied Physics Letters, 2009, 95, 231903.	3.3	4
210	Determination of liquidus temperature in Ti-rich alloys of the Fe–Ni–Ti system obtained by DTA, electrical conductivity and XRD measurements. International Journal of Materials Research, 2011, 102, 248-256.	0.3	4
211	Magnetic thermodynamics as proxy for chemical inhomogeneity in hemo-ilmenite solid solutions. Physics and Chemistry of Minerals, 2012, 39, 87-92.	0.8	4
212	Synthesis and characterization of Mg-based bulk metallic glasses in the Mg–Ag–Y–(Cu) system. Journal of Alloys and Compounds, 2021, 859, 157803.	5.5	4
213	X-ray Diffraction Computed Nanotomography Applied to Solve the Structure of Hierarchically Phase-Separated Metallic Glass. ACS Nano, 2021, 15, 2386-2398.	14.6	4
214	Atomic-Scale Characterization of Commensurate and Incommensurate Vacancy Superstructures in Natural Pyrrhotites. American Mineralogist, 2021, 106, 82-96.	1.9	4
215	The Besnus transition in 4C pyrrhotite revisited. Geophysical Journal International, 0, , .	2.4	4
216	Atomic structure evolution related to the Invar effect in Fe-based bulk metallic glasses. Nature Communications, 2022, 13, 1082.	12.8	4

0

#	Article	IF	CITATIONS
217	Thermally Decomposed Binary Fe–Cr Alloys: Toward a Quantitative Relationship Between Strength and Structure. Advanced Engineering Materials, 2022, 24, .	3.5	4
218	Identification of bulk metallic glass-forming compositions in La-based systems using ultrahigh gravitational acceleration. Acta Materialia, 2008, 56, 651-658.	7.9	3
219	Clustered field evaporation of metallic glasses in atom probe tomography. Ultramicroscopy, 2016, 162, 35-41.	1.9	3
220	Skyrmion lines, monopoles, and emergent electromagnetism in nanowires. , 2020, , 381-401.		3
221	Structural and Electronic Properties of Zr-Ti-Cu-Ni-Be Alloys. Materials Research Society Symposia Proceedings, 2000, 644, 191.	0.1	2
222	Comparison of the Decomposition and Crystallization Behavior of Zr and Pd Based Bulk Amorphous Alloys. Journal of Metastable and Nanocrystalline Materials, 2000, 8, 179-184.	0.1	2
223	Magnetism of nanostructured ferromagnets-experiments and theoretical model. Scripta Materialia, 2001, 44, 1425-1429.	5.2	2
224	Steep energy landscapes and adjustable magnetization states in a four-layer mean-field model with competing interactions. Physical Review B, 2012, 86, .	3.2	2
225	Structural relaxation in layered, non-stoichiometric Fe ₇ S ₈ . Physical Chemistry Chemical Physics, 2021, 23, 1165-1171.	2.8	2
226	Thermally Decomposed Binary Fe–Cr Alloys: Toward a Quantitative Relationship Between Strength and Structure. Advanced Engineering Materials, 0, , 2100909.	3.5	2
227	Recent progress in the area of bulk metallic glasses. International Journal of Materials Research, 2022, 97, 225-233.	0.3	2
228	Investigation of Nanocrystalline Fe by Small-Angle Neutron Scattering. Materials Science Forum, 1996, 207-209, 365-368.	0.3	1
229	Composition Dependence of Phase Separation and Crystallization in Deeply Undercooled Zr-(Ti-)Cu-Ni-Al Alloys. Materials Research Society Symposia Proceedings, 2000, 644, 561.	0.1	1
230	Testing of Frank's hypothesis on a containerless packing of macroscopic soft spheres and comparison with mono-atomic metallic liquids. Journal of Alloys and Compounds, 2011, 509, S60-S63.	5.5	1
231	Axis-selective excitation of gold nanoparticle resonances. Journal of the Optical Society of America B: Optical Physics, 2014, 31, 2621.	2.1	1
232	Eutectic isolation in Mg-Al-Cu-Li(-Y) alloys by centrifugal processing. Philosophical Magazine, 2003, 83, 2797-2813.	1.6	1
233	Metallic Glasses, Bulk. , 2003, , 1-12.		0

Plasmonic nanostructures made from aluminum fabricated by EUV interference lithography., 2007, , .

#	Article	IF	CITATIONS
235	XVII International Symposium on Metastable, Amorphous and Nanostructured Materials (ISMANAM) Tj ETQq1 1	0.784314 5.5	4 rgBT /Overlo
236	Comparison of conventional and Lorentz transmission electron microscopy in magnetic imaging of permanent magnets. Applied Physics Letters, 2021, 119, 022401.	3.3	0
237	Statistical and Thermodynamic Optimization of Trace-Element Modified Al-Mg-Si-Cu Alloys. , 2015, , 265-270.		0